N 84 - 1 8 8 3 8

Engine Cyclic Durability by Analysis and Material Testing

Albert Kaufman and Gary R. Halford
Lewis Research Center
Cleveland, Ohio

NASA

ENGINE CYCLIC DURABILITY BY ANALYSIS AND MATERIAL TESTING

Albert Kaufman and Gary R. Halford
NASA Lewis Research Center
Cleveland, Ohio 44135

SUMMARY

This paper addresses the problems of calculation of turbine engine component durability. Nonlinear, finite-element structural analyses, cyclic constitutive behavior models, and an advanced creep-fatigue life prediction method, Strainrange Partitioning, have been assessed for their applicability to the solution of durability problems in hot-section components of gas turbine engines. Three different component or subcomponent geometries are examined· a stress concentration in a turbine disk; a louver lip of a half-scale combustor liner; and a squealer tip of a first-stage high-pressure turbine blade. Cyclic structural analyses were performed for all three problems. The computed strain-temperature histories at the critical locations of the combustor liner and turbine blade components were imposed on smooth specimens in uniaxial, strain-controlled, thermomechanical cyclic tests to evaluate the structural and life analysis methods.

INTRODUCTION

Hot-section components of advanced aircraft gas turbine engines are exposed to extreme gas pressure and temperature environments. These operating conditions subject the combustor and high-pressure-stage turbine components to severe thermomechanical cycles that induce repeated inelastic straining and eventual fatigue cracking. Sophisticated analytical methods have been developed to assess the durability of the hot section components.

Nonlinear finite-element computer codes such as ANSYS (Ref. 1) and MARC (Ref. 2) have become available in recent years for calculating inelastic structural response under cyclic loading. The plasticity computations in these codes are based on classical incremental theory using a hardening model to define the yield surface under cycling, a yield criterion, and a flow rule. Generally, the von Mises yield criterion and the normality flow rule are used. Creep computations use a separate creep constitutive model that is not coupled to the plasticity model. Advanced life prediction methods, such as Strainrange Partitioning (Ref. 3), have been proposed for predicting low-cycle fatigue life from the stress-strain history at the critical location.

There is a need to calibrate these analytical methodologies against component experimental data to verify them and to guide their further development. Direct experimental verification from actual engine operation is difficult because the gas conditions are not generally known with sufficient accuracy, because the critical locations of these components are relatively inaccessible, and because the temperatures are beyond the high-temperature capability of state-of-the-art static strain gages. Without confidence in the reliability of the nonlinear structural analysis method or the ability to measure strains, it is seldom possible to verify the life prediction models under actual operating conditions. It is necessary, therefore, to verify these analytical methods with simpler experiments simulating the structural response of the engine component.

This paper addresses the problems of calculating turbine engine component durability. Three different component or subcomponent geometries are considered: a stress concentration in a turbine disk, a half-scale louvered combustor liner, and the squealer tip of a first-stage, high-pressure turbine blade. Nonlinear finite-element analyses, cyclic constitutive material behavior models, and advanced life prediction methods were assessed for their applicability to the solution of durability problems in these components.

Cyclic stress-strain response was obtained both experimentally (Ref. 4) and analytically (Ref. 5) for a two-dimensional representation of the disk notch problem. Three-dimensional nonlinear structural analyses were performed for a half-scale combustor liner (Ref. 6). This liner specimen was constructed in an identical configuration with current-service combustor liners. It was thermally cycled in an induction heated experimental rig. Three-dimensional nonlinear analyses were also performed for the tip region of an air-cooled turbine blade used in the first-stage, high-pressure turbine of a commercial aircraft engine (Ref. 7). This blade had a history of cracking in the squealer tip region. The mission cycle used for the blade analysis was based on full-scale engine factory durability testing.

The computed strain-temperature histories for the critical locations at the louver lip of the combustor liner and the squealer tip of the turbine blade were imposed on smooth specimens in uniaxial strain-controlled laboratory tests. Both structural and life analyses were performed for these thermomechanical test specimens and compared with experimental observations.

The disk notch testing program was a joint effort by the General Electric Co. and Louisiana State University under contract to NASA. Finite-element analyses of the

benchmark notch problems discussed in this paper were conducted at the NASA Lewis
Research Center. The combustor liner and blade tip durability studies were performed by
Pratt & Whitney Aircraft and the General Electric Co., respectively, under contract to
NASA.

DISK STRESS CONCENTRATION

Benchmark notch specimens with discontinuities representative of stress concentra-
tions in turbine disks were cyclically load tested to provide a body of experimental
strain measurements taken at the notch root for analytical verification purposes. The
specimen design is illustrated in Fig. 1. Specimens were fabricated from a nickel-base
turbine disk alloy (Inconel 718). It was not the intent of this program to cycle speci-
mens to failure nor make life prediction calculations.

Benchmark Notch Testing

The test program (Ref. 4) consisted of several axial load patterns, only two of
which are of interest herein (Fig. 2). All tests were conducted with a temperature
of 650° C maintained in the notch region. Testing was continued until cracks developed
or the tensile strain reached 1.6 percent, which was the limit that could be accommo-
dated by the measurement system. The load cycling for pattern I was not fully
reversed. However, the notch root strains were great enough that the local stress
response would tend toward a fully reversed condition with a mean stress of zero. The
frequency was 0.167 Hz. Monotonic step loading was applied for pattern II in five
increments, with a dwell time of approximately 1 hr for each increment.

Notch Strain Measurement

Notch root strains were measured with an interferometric strain displacement gage
(ISDG) that measures relative displacement between two small indentations at the center
of the notch root. These indentations are applied 100 μm apart with a Vickers hard-
ness tester. A schematic of the ISDG system is shown in Fig. 3.

The indentations were illuminated with monochromatic laser light, causing two
diffraction patterns to form. These diffraction patterns overlap, creating fringe
patterns that can be related to strain, as discussed in Ref. 4. The fringe patterns
were tracked by optical scanners. Fringes were recorded by a minicomputer which, in
turn, controlled the angular rotation of the scanners. The minicomputer converted the
fringe displacements to local notch root strains and stored the data on a diskette.

Finite-Element Analysis

A two-dimensional finite-element model of the specimen test section was con-
structed as shown in Fig. 4. Because of symmetry, only one-fourth of the test section
needed to be modeled. The model used 592 triangular elements, with a total of 335
nodes. Stress and total-plastic-creep strain distributions were obtained at the cen-
troids of the elements using the MARC nonlinear, finite-element computer program.

Cyclic yielding was determined from the stress-strain properties reported in Ref. 4
and the selected hardening model. Two hardening models, combined isotropic-kinematic
hardening and kinematic hardening, were selected for evaluation using load pattern I.
Monotonic stress-strain properties were used in conjunction with the combined model. A
bilinear representation of the saturated cyclic stress-strain curves was used for the
kinematic hardening model. The work hardening slope of the kinematic model was deter-
mined from energy considerations so that the strain energy would be identical with that
of the actual cyclic stress-strain curve. Each load cycle for load pattern I was sub-
divided into 30 increments. The analyses were terminated at the end of the second load
cycle.

Creep analyses were performed with the MARC program for the step loading sequence
of load pattern II. The creep properties given in Ref. 4 were correlated by a pre-
processor program into a functional relation in exponential form. The creep equations
were incorporated into MARC by means of a user subroutine. Creep analyses were per-
formed using both a strain hardening and a time hardening rule.

Comparison of Analyses and Experiments

In Fig. 5 analytical results using both combined and kinematic hardening models are
compared with the experimental load-notch strain cycle for load pattern I. Creep was
not a significant factor under the continuous cycling, isothermal load conditions of
this test. The experimental results demonstrated that a stable load-strain response
occurred on the first cycle with only minor strain changes in subsequent cycling. A
plasticity analysis using the combined hardening model did not accurately represent the
experimental results, it predicted, after initial loading, an elastic response with
further cycling (Fig. 5(a)). A second plasticity analysis using the kinematic hardening
model exhibited excellent agreement with the experimental results. The kinematic

hardening analysis predicted ratcheting between the first and second cycles and a stable notch strain cyclic response thereafter (Fig. 5(b)). Except for slightly overpredicting the ratcheting, these analytical results are consistent with the experimental cyclic response for load pattern I.

The results of the creep analyses for the step-loading sequence of load pattern II are compared with experimental results in Fig. 6. Agreement was good for initial loading and the first dwell time. However, on subsequent steps the analysis under-predicted the creep strains. The analysis was terminated after the third load step when it became obvious that the discrepancy between analysis and experiment was increasing. Essentially the same analytical results as shown in Fig. 6 were obtained using either strain hardening or time hardening rules.

The reason for the disagreement between experimental and analytical results in Fig. 6 is difficult to determine, as there was some question about the validity of the strain measurement for this test. When the specimen was completely unloaded after the last load step and then reloaded, only 60 percent of the previous total strain was measured. This implies that there was some drift in the displacement measurements during this test as a 40-percent strain recovery would be more than the combined plastic and creep strains before unloading.

HALF-SCALE COMBUSTOR LINER

Liner Durability Testing

An annular combustor liner specimen of the louver type of construction was subjected to thermal cycling in an induction heated experimental rig (Ref. 6). The specimen was half the scale of an actual combustor liner and was fabricated from the same material (Hastelloy X sheet). A conventional combustor liner of the louver type is shown in Fig. 7. The half-scale rig specimen consisted of five complete ring segments. The middle ring was the one studied in the experimental program. Using measured heat flux and cooling airflow rates as input, transient and steady-state, three-dimensional, heat-transfer analyses were conducted. The calculated temperature response (Fig. 8) of the middle louver of the liner specimen closely agreed with measured thermocouple data. The 90-sec test cycle consisted of a 20-sec transient from an isothermal minimum temperature of 504° C to a maximum temperature of 954° C, a 40-sec steady-state portion, and a cooldown back to the original isothermal condition. After the 20-sec heating transient, there was a temperature difference between the knuckle and louver lip of approximately 400° C. A total of 1730 cycles were accumulated on the test specimen. Thermal fatigue cracking was observed at the edge of the louver lip between 1000 and 1250 test cycles.

Finite-Element Analysis

The MARC nonlinear finite-element program, based on conventional tensile and creep properties of Hastelloy X, was used to calculate the structural response of the louver to the thermal cycling. For the analysis, each cycle was subdivided into 78 increments, consisting of 35 thermal load increments during heating, 14 creep increments during the steady-state dwell time, 25 thermal load increments during cooling, and four no-load increments during creep for residual load correction to ensure equilibrium.

A 0.5° segment between adjacent cooling holes was modeled with three-dimensional, 20-node isoparametric elements (Fig. 9). Full 27 Gaussian integration point elements were used around the cooling holes, while reduced integration elements with eight points were used for the remainder of the model to reduce computing time. To minimize round-off error due to the small included angle of the model segment, the program was run in double precision using 640 K words of storage on an IBM 370/3033 computer system. Each analytical cycle required approximately 45 min of execution time.

The effect of the complete shell structure was simulated by applying appropriate boundary conditions. Nodes along radial planes were constrained to move only in those planes. Additional boundary conditions were imposed to simulate the restraint of the fore and aft louvers of the test specimen by relating the nodal displacements of comparable points on the fore and aft louvers to the ratio of the original radii of these louvers.

Figure 10 shows the computed nonlinear stress-strain response at the louver lip critical location for two thermal cycles. Letter designations are given in Fig. 10 so that the response can be followed using the same letter designations given in Fig. 8. Initial yielding occurred on the first cycle after 5 sec heating (B) at a temperature of 732° C. Plastic flow took place between B and C. Creep analyses were conducted between 12.5 sec heating (C) and 60 sec (D) when the heating part of the cycle was completed. Reverse yield was reached 66 sec into the cycle, i.e., after 6 sec of cooling (E). Subsequent loading for the second cycle produced reyielding at a temperature of 893° C (B') as compared with 732° C (B) for the first cycle. The other points indicated for the second cycle (C' to F') occurred at similar times and temperatures as in the first cycle. The predicted stress-strain response had not stabilized after six cycles when the analysis was terminated. Cycles 3 to 6 exhibited similar stress-strain loops, which ratcheted in the negative strain direction. Each succeeding cycle had higher peak tensile stresses but an essentially constant strain range.

Smooth Specimen Simulation

To provide material response data for more direct evaluation of the creep-plasticity models used in the nonlinear analysis of the combustor liner, uniaxial thermomechanical testing was conducted on a smooth, cyclindrical specimen. The experimental system (Ref. 6) is capable of following a prescribed temperature-strain history. The predicted hoop mechanical strain and temperature history for the sixth loading cycle at the louver lip critical location was imposed on the uniaxial specimen. Since the edge of the louver lip experiences an essentially uniaxial stress field, the stress-strain response from the thermomechanical test is considered representative of the actual response producing fatigue failure.

The thermomechanical strain cycling demonstrated that the stress-strain response stabilized rapidly and that there were no significant peak stress changes after the first few cycles. Ratcheting was excluded by the imposed strain controlled test conditions. Reverse plasticity was observed during the cooling portion of the cycles. A MARC analysis was performed for a one-dimensional strain-controlled simulation of the experiment to investigate the ability of the creep-plasticity models to reproduce the experimental results. This analysis used the same material response models as the three-dimensional louver analysis and the same mechanical strain-temperature history as the uniaxial specimen test.

A comparison of the analytical results for the 15th and 30th cycles and the experimental results is shown in Fig. 11. The analytical stress-strain response did not stabilize and showed higher peak stresses than were obtained in the test. These discrepancies were attributed to the uncoupling of the creep and plasticity models. Improving the accuracy of the predicted stress-strain response under cyclic thermomechanical loading may require the use of one of the unified constitutive theories now undergoing development (Ref. 8).

Life Prediction

The cyclic stress-strain and temperature history determined from the structural analysis for the critical location at the louver liner was used directly as input into the life prediction calculations. Similarly, the measured cyclic response of the axially loaded thermomechanical test was used to calculate its probable lifetime and, hence, serve as an independent estimate of the predicted combustor liner life.

Although several advanced life prediction methods have been proposed over the past few years, this discussion is limited to only one, the Strainrange Partitioning (SRP) method of Ref. 3, because of its relative ease of application to the combustor liner durability problem. The life prediction calculations used isothermal SRP data generated at 870° C. This is justified since the SRP properties are not expected to be a significant function of temperature over the range of interest because the ductility of the Hastelloy X alloy is not significantly affected by temperature. Furthermore, only the results for PP (tensile plasticity reversed by compressive plasticity) and PC (tensile plasticity reversed by compressive creep) cycling are required since the hysteresis loop of interest contains only PP and PC components of inelastic strain range.

The inelastic strain range was calculated to be 0.10 percent for the sixth cycle of the finite-element analysis of the half-scale combustor liner. Of this, 0.0706 percent strain range was of the PC type and 0.0294 percent strain range was of the PP type. Hence, the interaction damage rule used in the SRP method for these conditions can be written as

$$1/N_{pred} = 0.706/N_{PC} + 0.294/N_{PP}$$

At an inelastic strain range of 0.10 percent at 870° C, N_{PC} = 7850 cycles to failure and N_{PP} = 10 600 cycles to failure (Ref. 6). The predicted life N_{pred} = 8500 cycles to failure for this case. This life is considerably greater than the 1000 to 1250 cycles to failure life observed for the half-scale combustor liner.

Applying the same calculational procedures to the prediction of the life of the axially loaded thermomechanical test specimen (which sustained a measured inelastic strain range of 0.12 percent), N_{pred} = 6300 cycles to failure. This predicted life is still considerably larger than the observed 1000 to 1250 cycle life of the liner. Although the thermomechanical fatigue specimen noted above was not cycled to failure, independent thermomechanical fatigue tests were conducted on axially loaded specimens of Hastelloy X at the Pratt & Whitney Aircraft Group in support of the combustor liner durability program. As an example, duplicate tests were conducted at 0.0167 Hz over the temperature range 427° to 927° C, out-of-phase (as the case herein), and the resultant inelastic strain ranges were 0.13 and 0.14 percent. Observed thermomechanical fatigue lives were 4944 and 4114 cycles to failure, respectively. Assuming the same fractional partitioning of the inelastic strain ranges of these two tests as for the sixth cycle of the finite-element analysis of the louver lip, the respective predicted lives are 5500 and 4950. Excellent agreement between thermomechanical experiment and prediction, based on isothermal SRP results, is realized in this case. The only discrepancy between predicted and observed lives is encountered for the half-scale component. Hence, some feature as yet to be identified, of the half-scale component, its method of testing, or its analysis must be responsible for the discrepancy. Clearly, the problem is not well

enough understood, and further research is required. Table I summarizes the life prediction results for the Hastelloy X alloy and the half-scale combustor liner.

AIR-COOLED TURBINE BLADE

Engine Durability Testing

The turbine blade under study has been used in the first-stage high-pressure turbine of a commercial aircraft engine. This blade is air-cooled and paired with an adjacent blade on a single three-tang dovetail. The airfoil has a span of 4.47 cm, a chord width of 3.30 cm, and a tip-to-hub radius ratio of 1.13.

A schematic of the blade and the tip region considered in the analysis is shown in Fig. 12. The material is a cast nickel-base superalloy, René 80, with a Codep-B aluminide coating. This blade was selected for study because of its significant creep-fatigue problems which induce cracking in the squealer tip of the blade above the tip cap. As these cracks grow, they cause coolant leakage and consequent overheating and loss of material from the blade tip. Engine efficiency then drops as tip clearances increase. Since centrifugal stresses are negligible near the blade tip, the cracking is primarily a thermal fatigue problem.

Figure 13 shows the mission cycle used for the analysis in terms of turbine inlet and compressor discharge temperatures and engine speed. This cycle is typical of an engine mission except for the condensed cruise time. High transient thermal stresses are induced during the engine takeoff acceleration and during thrust reversal. Creep mainly occurs during cruise between 6.7 sec (the end of acceleration) and 200 sec (the start of thrust reversal).

Metal temperatures were calculated from transient and steady-state, three-dimensional, heat-transfer analyses with known boundary conditions; these were in good agreement with thermocouple measurements from factory engine tests. The calculated metal-temperature, cycle-time profile for the critical tip location is shown in Fig. 14.

Engine durability testing was conducted at the factory to determine component fatigue life. The test cycle departed from a typical flight cycle in including two additional idle-to-takeoff transients per cycle to accelerate the test time. Their influence was accounted for in all life prediction calculations. At the end of 3000 stress-strain cycles (1000 missions) the blades were removed for inspection. All the blades tested were cracked at the blade tip critical location (Fig. 14); the cracks in all but one had progressed below the tip cap, which was 3.8 mm below the squealer tip.

Finite-Element Analysis

The ANSYS nonlinear computer program was used to perform the blade finite-element analysis. Temperature-dependent cyclic stress-strain and creep properties for René 80 alloy reported in Ref. 7 were used for the analysis. A kinematic hardening model was selected for the plasticity calculations, and a power law and a time hardening rule was used for the creep calculations.

Initially, the mission cycle was subdivided into 23 load increments. Inspection of the inelastic results for the first analytical cycle suggested that the number of increments could be reduced to six, provided that a sufficient number of iterations was permitted to ensure convergence of the plasticity solution. Rerunning the initial cycle with the reduced increments gave excellent agreement with the original analytical results. Time steps for the reduced load steps and some of the original load steps are indicated in Fig. 14.

The three-dimensional, finite-element model of the blade tip region above the 75 percent span position is shown in Fig. 15. A total of 580 eight-node isoparametric elements with 1119 nodes was used to model the airfoil shell, squealer tip, tip cap, and ribs. The eight-node element was used because the 16- and 20-node solid elements in ANSYS lacked creep capabilities. Boundary conditions were applied to constrain all nodes at the base of the model to lie on the 75-percent plane of the airfoil. The span length of the model was sufficient to preclude interference of the applied boundary conditions with the stress-strain solution at the squealer tip. Additional boundary conditions were applied to prevent rigid body motion on the 75-percent plane.

Figure 16 shows the stress-strain response at the critical location from the ANSYS nonlinear analysis for the first, second, and seventh mission cycles. Letter designations are given on the hysteresis loops which are consistent with those on the temperature-time response of Fig. 14. Plasticity analyses were performed for the heating portion of the cycle from A to B, and creep analyses during the relatively steady-state portion from B to C. The remainder of the cycle from C to D involved primarily elastic response. As shown in Fig. 16, continued cycling produces ratcheting of the hysteresis loops in the negative strain direction with progressively higher peak tensile stresses during cooling. Although complete stabilization of the hysteresis loops was not achieved when the analysis was terminated after the seventh cycle, the creep strain change per cycle had diminished to less than 35 μin/in for the last

cycle. The computed total strain range per cycle increased from 3082 to 3089 micro-strain between the first and seventh cycles, a change of less than 0.3 percent.

Smooth Specimen Simulation

As in the combustor liner study, the validity of the nonlinear analysis was evaluated by means of a uniaxial, thermomechanical test of a smooth, cylindrical specimen. The experimental system which can follow a prescribed strain-temperature history, is described in Ref. 7. The total strain and temperature history at the critical location from the seventh cycle of the ANSYS blade analysis defined the specimen test conditions. An ANSYS analysis was performed for this uniaxial test using the same material properties and creep-plasticity models as the blade analysis.

A comparison of the analytical results for the seventh cycle with the stable test cycle is shown in Fig. 17. The test demonstrated more rapid stabilization of the stress-strain response and a higher tensile peak stress than was predicted by the nonlinear analysis. On the initial cycle, the stress relaxation exhibited in the test was approximately three times greater than that shown by the analysis. These discrepancies between analysis and experiment could also be caused by the uncoupling of the creep and plasticity models. The NASA Lewis Research Center has instituted programs under its turbine engine Hot-Section Technology Project to develop unified constitutive models that will more realistically represent material cyclic behavior by coupling time-dependent and time-independent inelastic strains and avoiding other simplifying assumptions of classical plasticity.

Life Prediction

Similar life prediction procedures as were used for the combustor liner were used to predict the thermal fatigue lifetime of the René 80 turbine blades. The SRP life prediction method was used in conjunction with the ductility normalized (DN) SRP life relations (Ref. 9). Since the ductility of René 80 is a strong function of the temperature, the DN-SRP life relations enable the expected temperature-dependent SRP life relations to be determined from tensile ductility information. Lives were calculated for the blade tip and for the thermomechanically loaded test specimen used in simulating the cyclic stress-inelastic strain response at the critical location. The thermomechanically loaded test specimen was not carried to failure.

Any effects of the aluminide coating on fatigue life were ignored in the calculations presented herein. SRP characterization results and ductility data for René 80 over the temperature regime of interest were obtained from Ref. 7.

Results of the structural analysis and of the measurements made on the axially loaded thermomechanical test specimen revealed that the inelastic strain range was essentially composed of only the PC type strain range. Therefore, the interaction damage rule reduces to the simple statement that the predicted life, N_{pred} is equal to the PC lifetime, N_{PC}. For the temperature conditions existing at the critical crack initiation location on the blade tip, the PC life relation (ascertained from isothermal data at 1000° C plus modification according to the DN-SRP life relations to account for property variations caused by temperature) for René 80 (Ref. 7) is,

$$N_{pred} = N_{PC} = 5.0(\Delta\varepsilon_{PC})^{-1.56}$$

For $\Delta\varepsilon_{PC} = 0.013$ percent as calculated from the ANSYS analysis, $N_{pred} = 4420$ cycles to failure. For the thermomechanically loaded test specimen, $\Delta\varepsilon_{PC} = 0.030$ percent and $N_{pred} = 1200$ cycles to failure. The observed blade tip life was 3000 cycles to failure and is bracketed by the 1200 and 4420 cycle-to-failure predictions of life. Thus, for the blade tip durability problem discussed herein, the hardware lives can be reasonably predicted from the isothermal SRP properties. The reasonably good agreement was obtained, however, only after having modified the 1000° C isothermal SRP life relation for PC straining to account for the substantially lower straining capacity of René 80 at the low temperature end of the thermal cycle. The life prediction results for the René 80 and the turbine blade are shown in Table I.

SUMMARY OF RESULTS

The results of the durability studies of engine hot-section components can be summarized as follows·

1. The nonlinear finite-element structural analyses indicated that the uncoupled creep and plasticity models did not give an accurate representation of the cyclic thermomechanical response of the structures. Tests of uniaxial, strain-controlled specimens with the same strain-temperature histories as computed at the combustor liner and turbine blade failure locations stabilized rapidly. Analytical simulations of these experiments incorrectly exhibited continued cyclic hardening with increasing peak tensile stresses.

2.   Analysis of the disk notch problem using kinematic hardening showed excellent agreement with experimental results for continuous load cycling. However, creep analyses of this specimen predicted strains that were low compared with strain measurements under monotonic step loading. It is uncertain whether this disagreement is due to the inadequacy of the creep model or to measurement errors.

3.   Life predictions based on isothermal Strainrange Partitioning characteristics and results of the inelastic structural analyses overpredicted the fatigue lives of the half-scale combustor liner and turbine blade tip. The degree of overprediction was not great for the turbine blade tip problem (4420 cycles predicted versus 3000 cycles observed), but substantial error was encountered for the combustor liner problem (8500 cycles predicted versus 1000 to 1250 cycles observed).

4.   Life predictions based on isothermal Strainrange Partitioning characteristics were also applied to a few axial strain-controlled, thermomechanical fatigue tests conducted on the combustor liner material. Excellent agreement was obtained between predicted (4950 and 5500 cycles) and observed (4144 and 4944 cycles, respectively) lives for the thermomechanical tests.

5.   The significant overprediction of life of the half-scale combustor liner apparently is associated with some feature (as yet unidentified) of the hardware, the method of testing, or the method of analysis.

REFERENCES

1.   Kohnke, P. C.· ANSYS Engineering Analysis System Theoretical Manual. Houston, PA, Swanson Analysis Systems, Inc., Nov. 1977.
2.   MARC General Purpose Finite Element Analysis Program. User Manual, Vol. A: User Information Manual and Vol. B: Marc Element Library. Palo Alto, CA, MARC Analysis Research Corp., 1981.
3.   Characterization of Low Cycle High Temperature Fatigue by the Strainrange Partitioning Method. AGARD-CP-243, London, Technical Editing and Reproduction Ltd., 1978.
4.   Domas, P. A., et al.· Benchmark Notch Test for Life Prediction. (R82AEB358, General Electric Co., NASA Contract NAS3-22522.) NASA CR-165571, 1982.
5.   Kaufman A.: Evaluation of Inelastic Constitutive Models for Nonlinear Structural Analysis. Nonlinear Constitutive Relations for High Temperature Applications. NASA CP-2271, 1983, pp. 89-105.
6.   Moreno, V.: Combustor Liner Durability Analysis. (PWA-5684-19, United Technologies Corp., Pratt & Whitney Group; NASA Contract NAS3-21836.) NASA CR-165250, 1981.
7.   McKnight, R. L.; Laflen J. H., Halford, G. R., and Kaufman, A.: Turbine Blade Nonlinear Structural and Life Analysis. J. Aircr., Vol. 20, No. 5, May 1983, pp. 475-480.
8.   Walker, K. P.· Research and Development Program for Nonlinear Structural Modeling with Advanced Time-Temperature Dependent Constitutive Relationships. (PWA-5700-50, United Technologies Research Center, NASA Contract NAS3-22055.) NASA CR-165533, 1981.
9.   Halford, G. R., Saltsman, J. F., and Hirschberg, M. H.· Ductility-Normalized Strainrange Partitioning Life Relations for Creep-Fatigue Life Predictions. Environmental Degradation of Engineering Materials, Blacksburg, VA, Virginia Tech Printing Department, Virginia Polytechnic Institute and State University, 1977, pp. 599-612.

TABLE 1. - SUMMARY OF LIFE PREDICTION RESULTS

Structure	Material	Temperature range, °C	Frequency, Hz	Inelastic strain range, percent	Observed life, cycles	Predicted SRP life, cycles
Combustor liner[a]	Hastellov X	504 - 904	0.0111	0.10	1000 - 1250	8500
Axially loaded[b] thermomechanical specimens	Hastelloy X	504 - 904 427 - 927 427 - 927	0.0111 .0167 .0167	0.12 .13 .14	---- 4944 4114	6300 5500 4950
Turbine blade tip[c]	René 80	344 - 1000	0.0049	0.013	3000	4420
Axially loaded[b] thermomechanical specimen	René 80	344 - 1000	0.0049	0.030	----	1200

[a]Sixth cycle of finite element analysis.
[b]Out-of-phase cycle (maximum temperature at minimum strain).
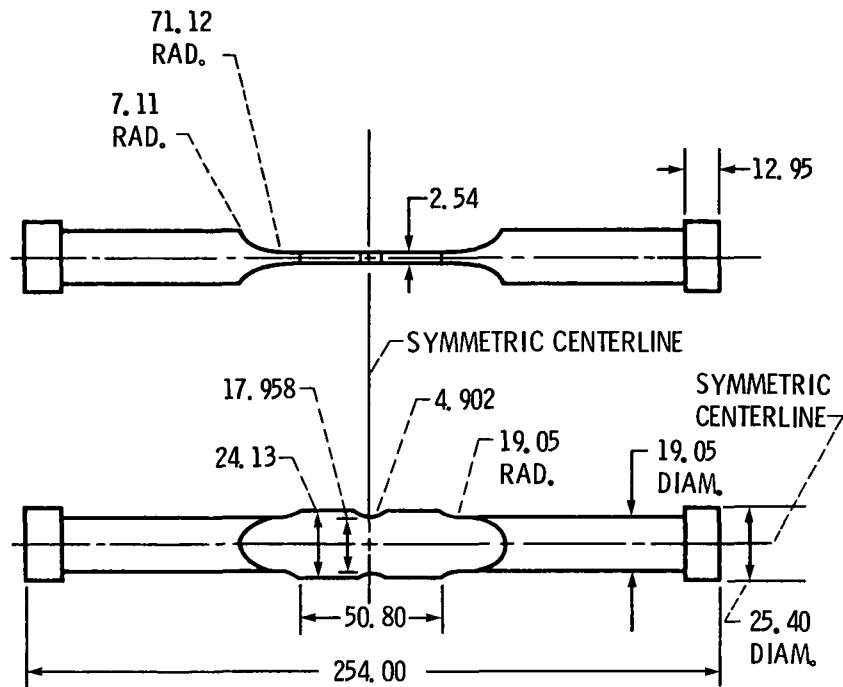[c]Seventh cycle of finite element analysis.

TABLE 1. - SUMMARY OF LIFE PREDICTION RESULTS

Structure	Material	Temperature range, °C	Frequency, Hz	Inelastic strain range, percent	Observed life, cycles	Predicted SRP life, cycles
Combustor liner[a]	Hastelloy X	504 - 904	0.0111	0.10	1000 - 1250	8500
Axially loaded[b] thermomechanical specimens	Hastelloy X	504 - 904 427 - 927 427 - 927	0.0111 .0167 .0167	0.12 .13 .14	---- 4944 4114	6300 5500 4950
Turbine blade tip[c]	René 80	344 - 1000	0.0049	0.013	3000	4420
Axially loaded[b] thermomechanical specimen	René 80	344 - 1000	0.0049	0.030	----	1200

[a]Sixth cycle of finite element analysis.
[b]Out-of-phase cycle (maximum temperature at minimum strain).
[c]Seventh cycle of finite element analysis.

Fig. 1. - Benchmark notch specimen (K_t = 1. 9). (Dimensions in mm.)

(a) Pattern I.

(b) Pattern II.
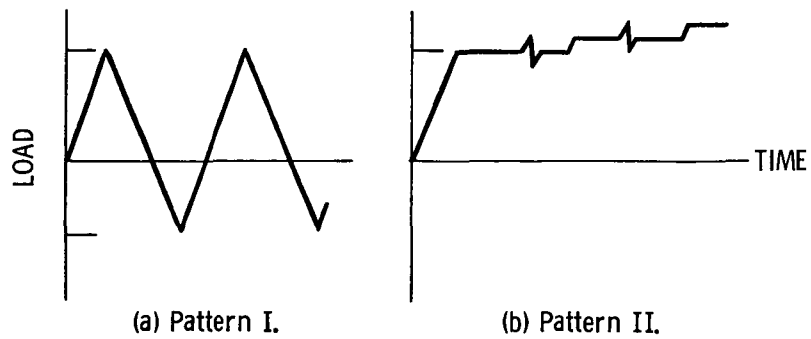
Fig. 2. - Load spectra for benchmark notch specimen.
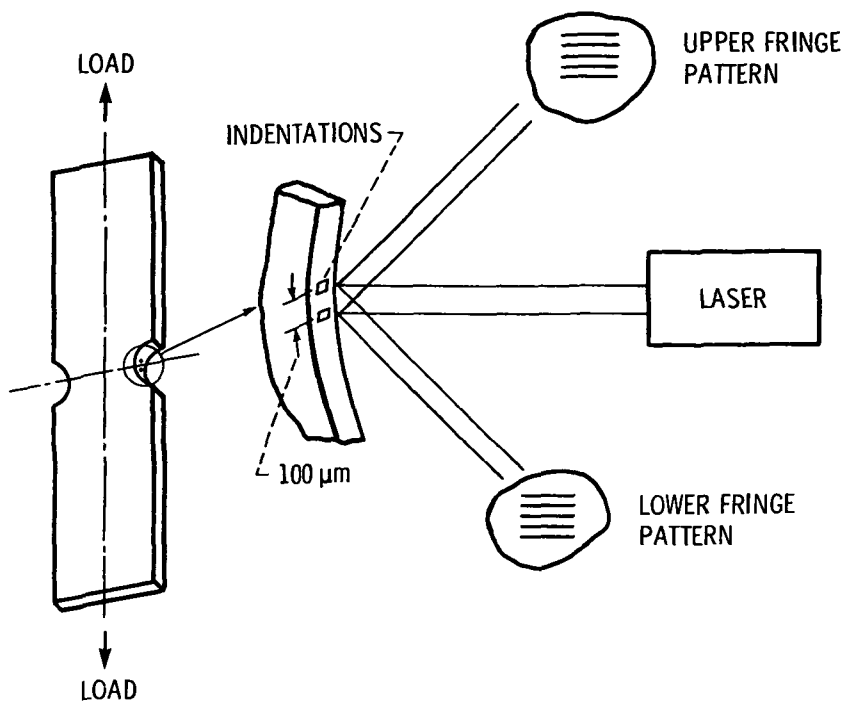
Fig. 3. – Schematic of ISDG.
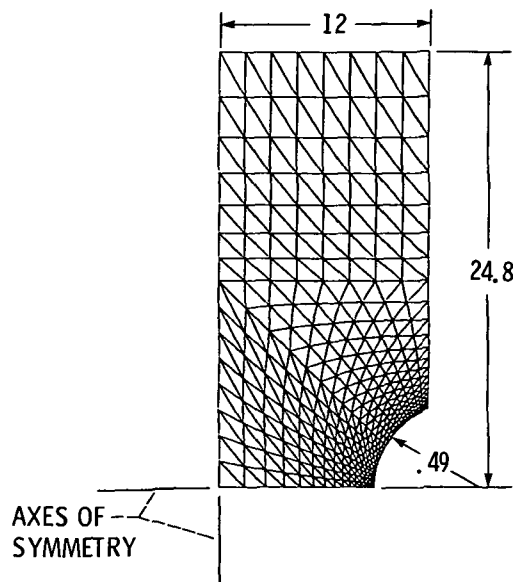
Fig. 4. – Benchmark notch specimen finite-element model. (Dimensions in mm.)
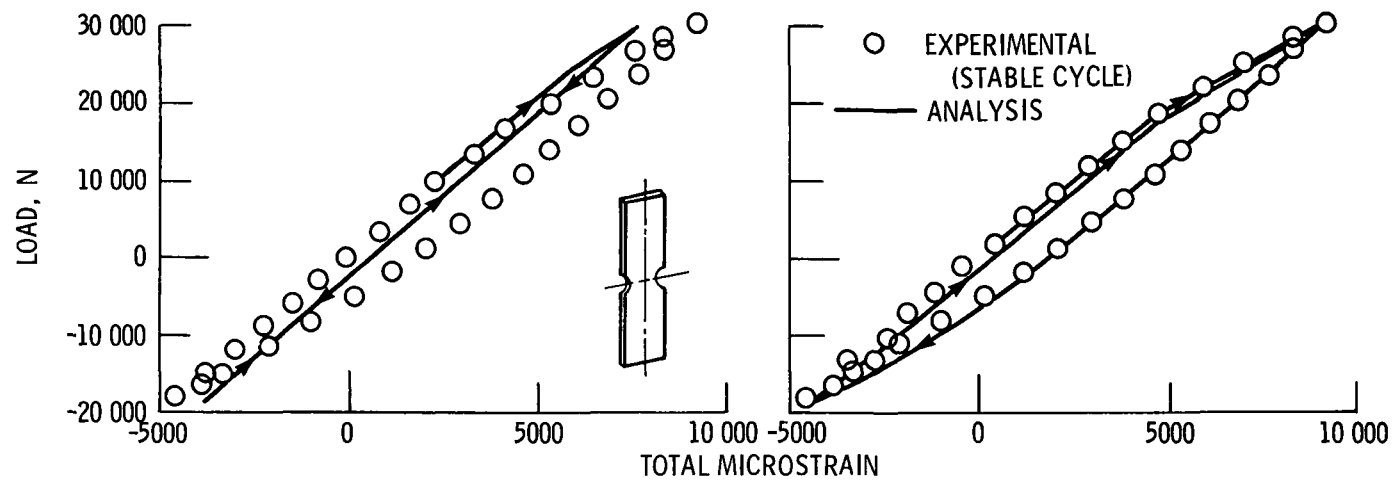
(a) Combined model.   (b) Kinematic model.

Fig. 5. – Comparison of benchmark notch specimen experimental and analytical results for load pattern I.
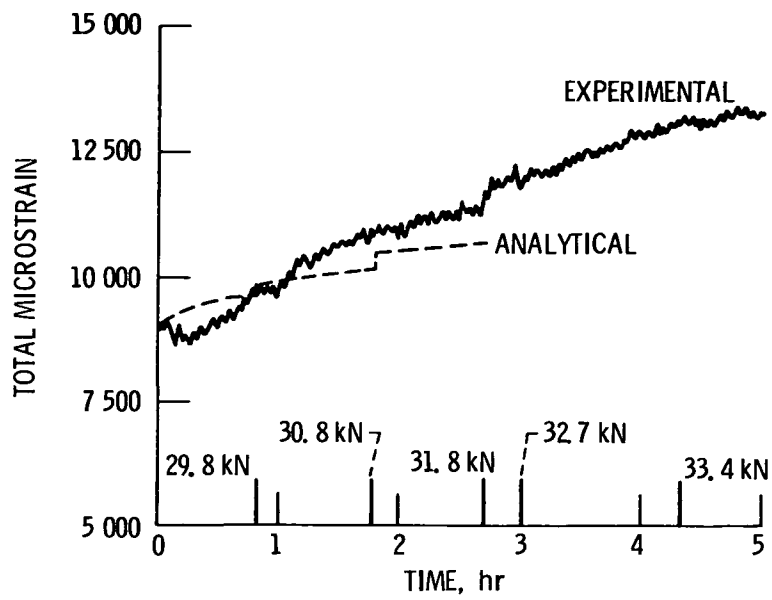
Fig. 6. - Comparison of benchmark notch specimen experimental and analytical results for load pattern II.
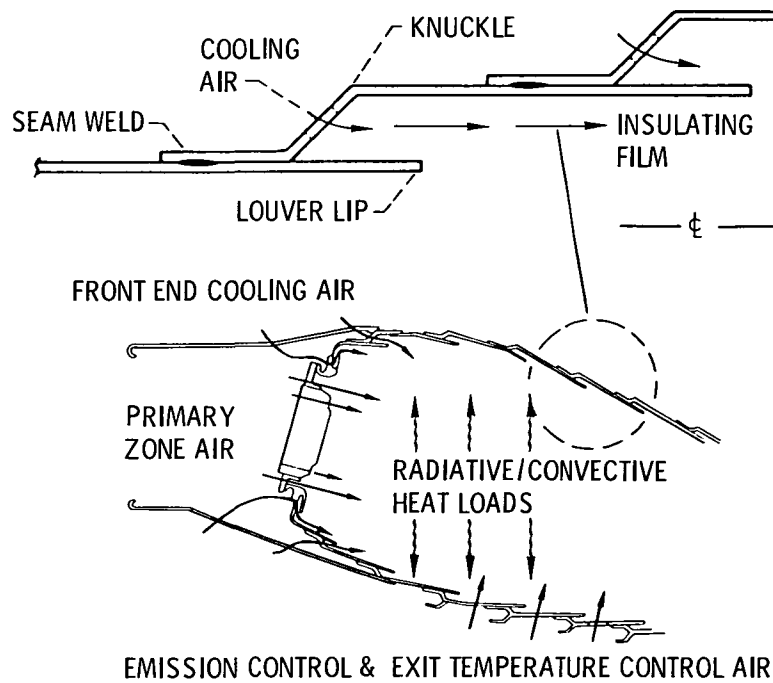
Fig. 7. - Typical louver combustor liner construction and airflow distribution.
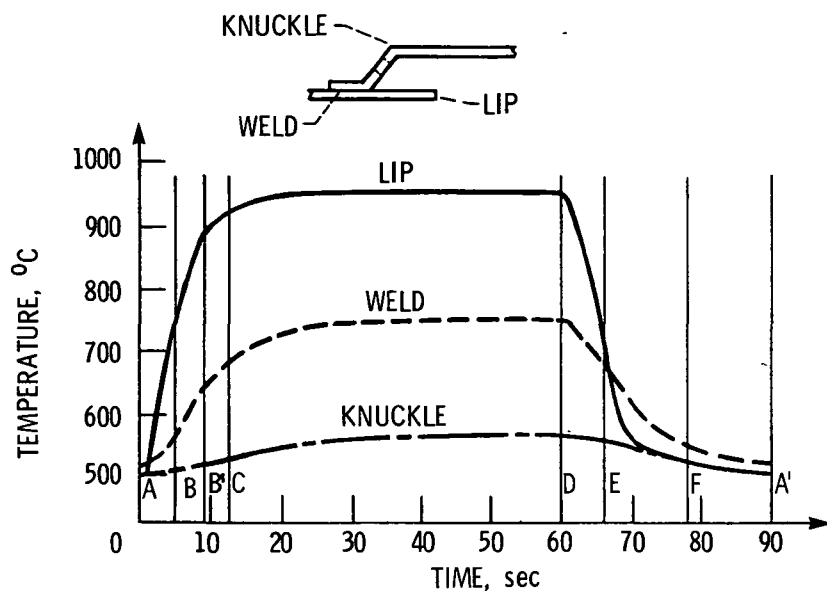
Fig. 8. – Louver temperature response.
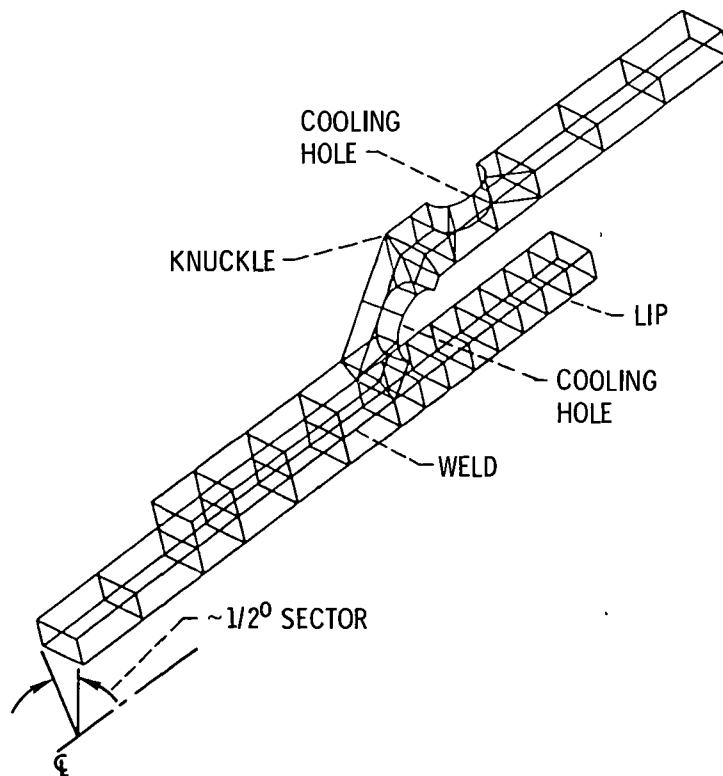
Fig. 9. – Combustor liner finite-element model.
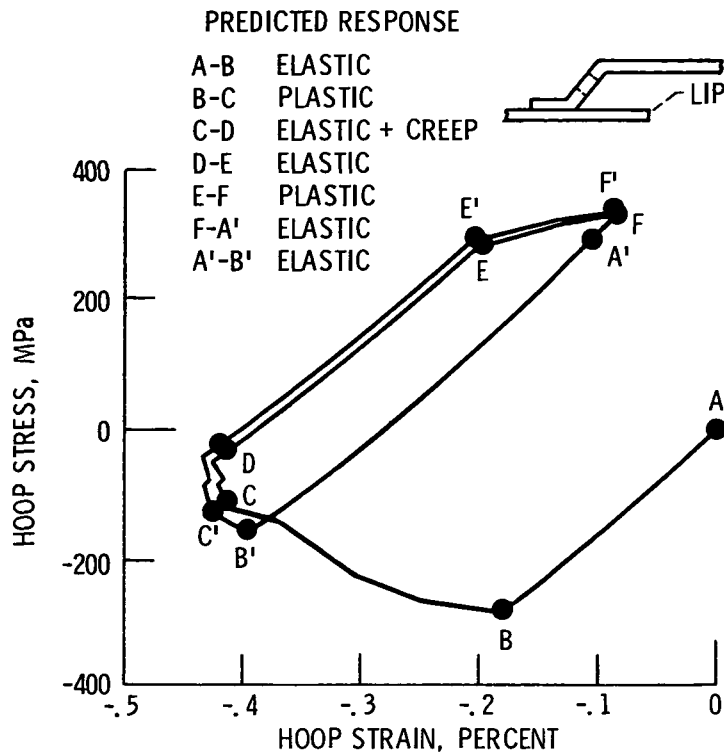
Fig. 10. - Nonlinear analysis stress-strain response at louver lip of combustor liner.
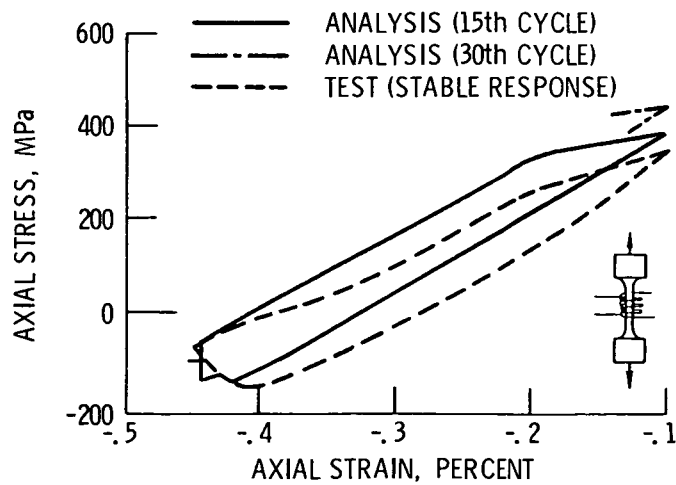
Fig. 11. - Comparison of uniaxial thermomechanical test and analytical results for combustor liner simulation.
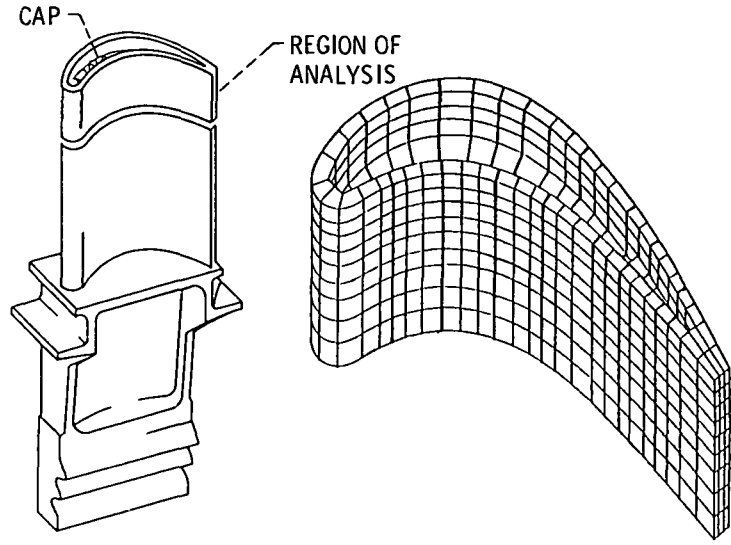
Fig. 12. - First-stage high-pressure turbine blade and finite-element model.

□ TURBINE INLET
○ COMPRESSOR DISCHARGE

(a) Turbine inlet discharge temperatures.

(b) Core engine speed.
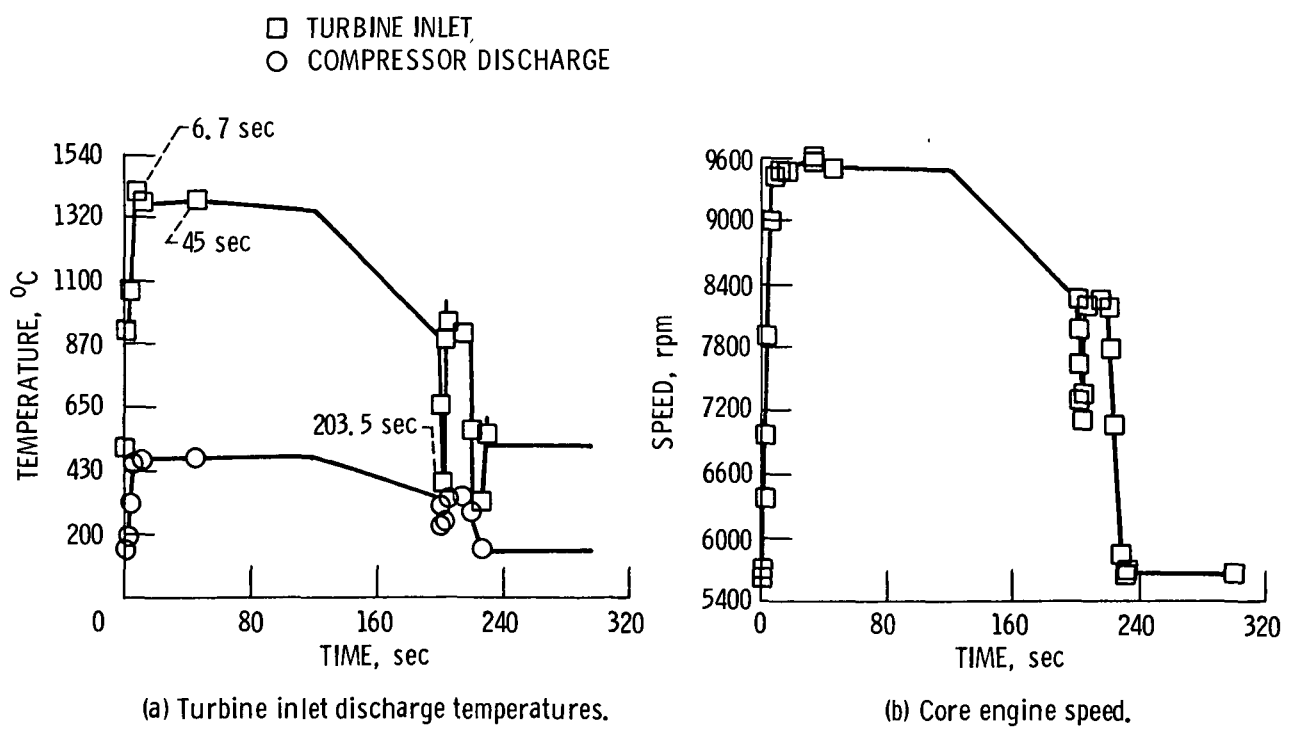
Fig. 13. - Mission cycle used for analysis of turbine blade.
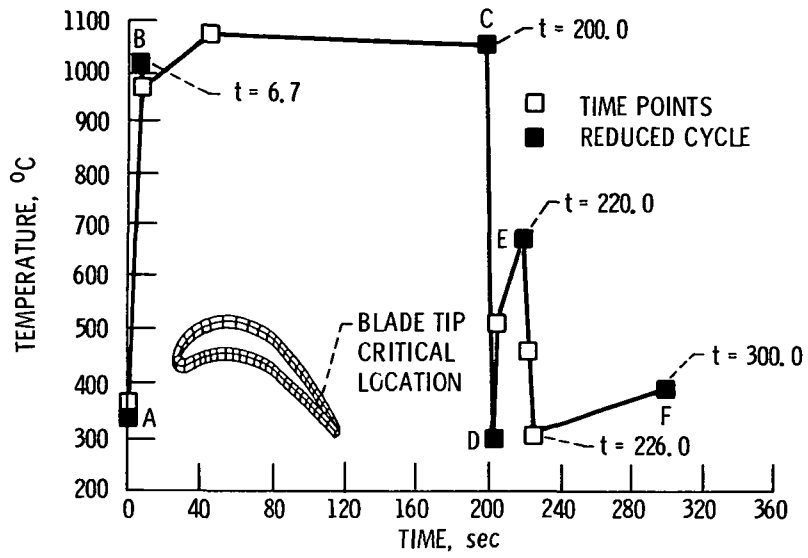
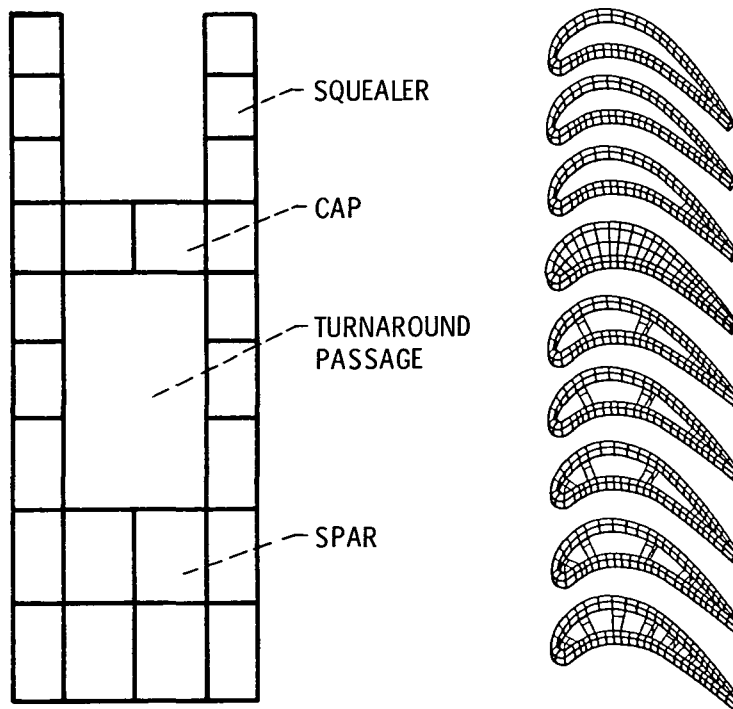Fig. 14. - Blade metal temperature response at critical location.

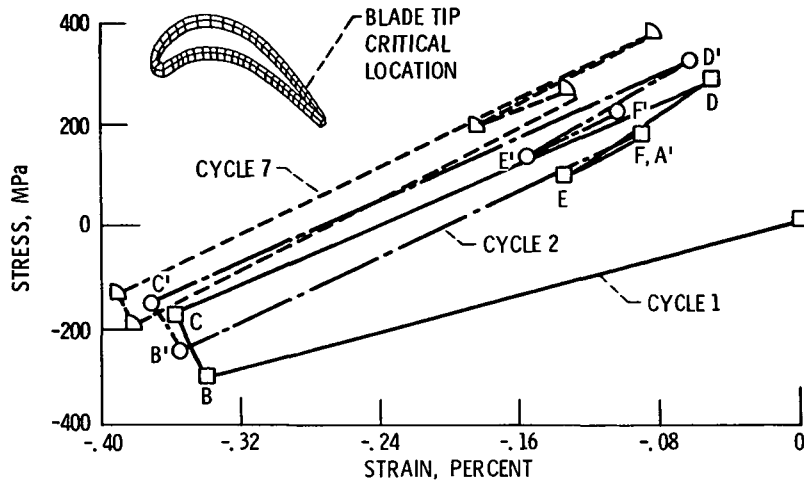Fig. 15. - Finite-element model of blade tip.

Fig. 16. – Inelastic analysis results: stress-strain response at critical location of turbine blade.
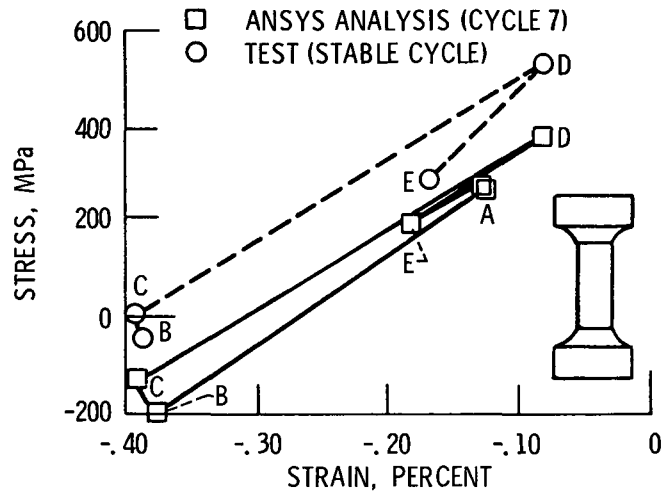

Fig. 17. – Comparison of uniaxial thermome-chanical test and inelastic analysis results for turbine blade simulation.

1. Report No. NASA TM-83577	2. Government Accession No.	3. Recipient's Catalog No.
4. Title and Subtitle Engine Cyclic Durability by Analysis and Material Testing		5. Report Date
		6. Performing Organization Code 505-33-12
7. Author(s) Albert Kaufman and Gary R. Halford		8. Performing Organization Report No. E-1964
		10. Work Unit No.
9. Performing Organization Name and Address National Aeronautics and Space Administration Lewis Research Center Cleveland, Ohio 44135		11. Contract or Grant No
		13. Type of Report and Period Covered Technical Memorandum
12. Sponsoring Agency Name and Address National Aeronautics and Space Administration Washington, D.C. 20546		14. Sponsoring Agency Code

15. Supplementary Notes

16. Abstract

This paper addresses the problem of calculation of turbine engine component durability. Nonlinear, finite-element structural analyses, cyclic constitutive behavior models, and an advanced creep-fatigue life prediction method, Strainrange Partitioning, have been assessed for their applicability to the solution of durability problems in hot-section components of gas turbine engines. Three different component or subcomponent geometries are examined: a stress concentration in a turbine disk; a louver lip of a half-scale combustor liner; and a squealer tip of a first-stage high-pressure turbine blade. Cyclic structural analyses were performed for all three problems. The computed strain-temperature histories at the critical locations of the combustor linear and turbine blade components were imposed on smooth specimens in uniaxial, strain-controlled, thermomechanical fatigue tests to evaluate the structural and life analysis methods.

17. Key Words (Suggested by Author(s)) Turbine engines; Life (durability); Thermal fatigue; Structural analysis; Constitutive equations; Creep-fatigue	18. Distribution Statement Unclassified - unlimited STAR Category 39		
19. Security Classif. (of this report) Unclassified	20. Security Classif. (of this page) Unclassified	21. No. of pages	22. Price*

National Aeronautics and
Space Administration

Washington, D.C.
20546

SPECIAL FOURTH CLASS MAIL
BOOK

NASA

POSTMASTER: If Undeliverable (Section 158
Postal Manual) Do Not Return